New Density Functional Approach for Solid-Liquid-Vapor Transitions in Pure Materials

Gabriel Kocher and Nikolas Provatas
Department of Physics, Centre for the Physics of Materials, McGill University, Montreal, Quebec H3A 2T8, Canada

(Received 28 December 2014; published 15 April 2015)

A new phase field crystal (PFC) type theory is presented, which accounts for the full spectrum of solid-liquid-vapor phase transitions within the framework of a single density order parameter. Its equilibrium properties show the most quantitative features to date in PFC modeling of pure substances, and full consistency with thermodynamics in pressure-volume-temperature space is demonstrated. A method to control either the volume or the pressure of the system is also introduced. Nonequilibrium simulations show that 2- and 3-phase growth of solid, vapor, and liquid can be achieved, while our formalism also allows for a full range of pressure-induced transformations. This model opens up a new window for the study of pressure driven interactions of condensed phases with vapor, an experimentally relevant paradigm previously missing from phase field crystal theories.

DOI: 10.1103/PhysRevLett.114.155501 PACS numbers: 81.10.Aj, 81.10.Bk, 81.10.Dn, 81.15.Aa

In the study of materials, modeling nonequilibrium phase transformations is crucial and requires capturing atomic length features, while remaining consistent with Thermodynamics at long length and time scales. Toward this goal, phase field crystal (PFC) modeling [1] has recently emerged as an efficient and mathematically accessible option, incorporating the thermodynamics of phase transformations and most salient solid state properties, including elastoplastic deformations and grain boundaries, all on diffusive time scales [2]. Extensions to the original model have been applied to complex structural transformations in pure materials [3,4], multicomponent alloys [5], and the study of solid-liquid and solid-solid transformations [6–8].

To date, however, most PFC modeling has considered only liquid-solid or solid-solid transitions at fixed average density, a situation that severely precludes the applicability of the PFC paradigm to problems related to the interaction of condensed phases with vapor. A method to model such systems was introduced [9], but it is not derived from a single order parameter and precludes a description of the critical point. In this Letter, we introduce a new, more fundamental PFC-type theory of pure substances, which accounts for the full spectrum of solid-liquid-vapor transitions within the framework of a single density order parameter. Our formalism is shown to be fully consistent with thermodynamics in pressure-volume-temperature space, while inheriting the features of previous PFC models. It also naturally accounts for different anisotropies and nucleation barriers for vapor-solid and liquid-vapor systems. We additionally introduce a method to control either the volume or the pressure of the system. As a demonstration, we show an application in pressure-driven phase transformations.

Consider classical density functional theory (c-DFT) [10,11]: Let $\rho(\mathbf{r})$ be a field representing the atomic density of an interacting liquid. The free energy of such a liquid is generally written as $F_{cdft}[\rho]/(k_BT) = F_{id}[\rho] + \Phi[\rho]$ where F_{id} is the energy of an ideal gas and Φ the contribution due to interactions. Φ is then treated by functional expansion around a reference density $\bar{\rho}$, in a power series of $n = (\rho - \bar{\rho})/\bar{\rho}$, and interactions are described by a sequence of n-point correlations $C^{(n)}(\mathbf{r}_1, .., \mathbf{r}_n)$. While these correlation functions are not known in general, a truncation of the series to second order along with a suitable ansatz of $C^{(2)}$ has been shown to separately describe both vapor-liquid interfaces [12] or solidification problems [10] with success. PFC methods additionally rely on an expansion of the ideal free energy around $n \sim 0$, to create what one may call a "smooth atom" approximation [13–16] of an atomic density field. While the atomic density interpretation is lost, the order parameter field n still exhibits spatial variations and retains numerous crucial features of the c-DFT atomic density.

To overcome the limitations of two-point correlations on multiphase behavior, we introduce here a theory that relies on higher order correlations. Consider the van der Waals theory for the liquid vapor transition [17]. Its improvement to the ideal gas law is based on two simple mean-field postulates: the attraction between particles is proportional to the average surrounding density, and each particle proportionally reduces the free volume available to other particles. At the field theory level for the spatially varying coarse grained field ρ, such improvements can be described by the free energy $F_{VdW}[\rho]/(k_BT) = F_{id} - \int d\mathbf{r}[\rho_{mf}\ln(1-\rho_{mf}b) + (a/k_BT)\rho_{mf}^2]$, where $\rho_{mf}(\mathbf{r}) = \int d\mathbf{r}\chi(\mathbf{r}-\mathbf{r}')\rho(\mathbf{r})$ is a local spatial average of the density field ρ, with χ a local smoothing kernel. In the limit of a fully uniform field, setting $\rho = \rho_{mf} = N/V$ reduces this free energy to the standard van der Waals free energy, where a and b, respectively, control the magnitude of the attraction and repulsion between atoms. This formulation lends itself to an interesting c-DFT interpretation. Indeed, expanding it around a reference density generates a power series in ρ_{mf}, that we may interpret as a series of correlation functions. In the following, we introduce a formulation that incorporates all the qualitative contributions from the van der Waals theory into the free energy of the standard PFC-expanded formalism. In addition of an expanded ideal free energy, it contains both a sharp two-point kernel and a set of long-range kernels, which allow for the description of solid, liquid, and vapor phases from a single microscopic order parameter field.

Our model uses the following free energy functional ($\mathcal{F} = F/\bar{\rho}k_BT$):

$$\begin{aligned}\mathcal{F}[n] = &\int d\mathbf{r}\left[\frac{n(\mathbf{r})^2}{2} - \frac{n(\mathbf{r})^3}{6} + \frac{n(\mathbf{r})^4}{12}\right]\\ &-\frac{1}{2}\int d\mathbf{r}_1 d\mathbf{r}_2 C^{(2)}(\mathbf{r}_1 - \mathbf{r}_2)n(\mathbf{r}_1)n(\mathbf{r}_2)\\ &+\sum_{m=3}^{4}\frac{1}{m}\left[\int d\mathbf{r}_1..d\mathbf{r}_m\chi^{(m)}(\mathbf{r}_1,..,\mathbf{r}_m)n(\mathbf{r}_1)..n(\mathbf{r}_m)\right].\end{aligned} \tag{1}$$

The first line results from the expansion of the ideal gas free energy $F_{id}[\rho]$, while the second line adds a multipeaked two-point correlation function. The choice of the latter term determines the structure and properties of the solid phase. While elaborate choices can be made for this term (to target specific 2D or 3D structures [3,4]), for simplicity, we choose a kernel that yields triangular (bcc) structures in 2D (3D) [1]: $C^{(2)}(\mathbf{r}_1 - \mathbf{r}_2) = 1 - r - B_x(1 - \nabla^2)^2$. Here, B_x controls both the bulk compressibility and the strength of the anisotropy in the periodic phase, while r acts as an effective temperature parameter. Vapor-liquid transformations are controlled by the $\chi^{(3)}$ and $\chi^{(4)}$ functions. These are effective three- and four-point correlation functions, given by $\chi^{(3)} = (ar + b)\chi(\mathbf{r}_1 - \mathbf{r}_2)\chi(\mathbf{r}_1 - \mathbf{r}_3)$ and $\chi^{(4)} = c\chi(\mathbf{r}_1 - \mathbf{r}_2)\chi(\mathbf{r}_1 - \mathbf{r}_3)\chi(\mathbf{r}_1 - \mathbf{r}_4)$, with $\chi(k) = \exp[-k^2/(2\lambda)]$ in reciprocal space. χ affects low $\mathbf{k}$ modes, only picking up density contributions at long wavelengths. The a, b, and c parameters determine the bulk properties of the uniform phases, while λ affects surface energetics. We present the qualitative physics of the model here, while the study of interface energies will be discussed elsewhere.

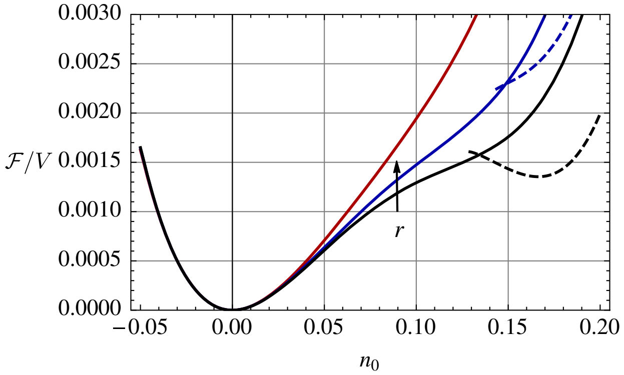

FIG. 1 (color online). Two-dimensional free energy landscapes (vs average density) for different effective temperatures r. Uniform phases: continuous lines, periodic phases: dashed. Black: $r = 0.14$, blue: $r \approx 0.148$ (triple point), red: $r = 0.17$. Other parameters: $a = 50$, $b = -19$, $c = 50$, $B_x = 0.7$.

Substituting a uniform $n(\mathbf{r}) = n_0$ into Eq. (1) yields a Landau free energy in terms of n_o for uniform phases (liquid or vapor). This is shown in Fig. 1. For simplicity, only 2D results are presented here. For nonzero a, b, and c parameters, at low enough rescaled temperature r, a double well landscape sets in between liquid and vapor. The definition of pressure, $\mathcal{P} = -(\mathcal{F}/V - \mu n_0)$, gives the bulk moduli of the uniform phases $\beta = n_0(\partial\mathcal{P}/\partial n_0)$. The vapor and liquid bulk moduli can be made different by several orders of magnitude, consistent with physical systems. For the parameter $r = 0.15$, $\beta_{\text{liq}} \sim 10^{-3}$ in the liquid region, while in the vapor region, β_{gas} varies between $\sim 10^{-4}$ in coexistence to $\sim 10^{-6}$ near $n_0 \sim 0.001$. β vanishes as the critical point is approached, where the compressibility diverges with an exponent of $(r - r^*)^{-1}$. The periodic phase of the functional is treated via a one-mode approximation [1], leading to a Landau theory in both the average density and the amplitude of the solid. Minimizing out the amplitudes gives the solid free energy, a few examples of which are also plotted in Fig. 1. The phase diagram can be computed by performing common tangent constructions on the Landau theory for different pressures. Figure 2(a) shows the density-temperature-pressure phase diagram of Eq. (1). It features solid-liquid, solid-vapor, and vapor-liquid coexistence regions, and is in excellent qualitative agreement with experimental phase diagrams for pure materials [17,18]. The vapor-liquid phase separation is parabolic, due to the expanded nature of the theory. Higher order long range correlation terms may be added systematically to fine-tune this behavior. The pressure-temperature phase diagram [Fig. 2(b)] also shows a behavior consistent with experiments. Along with the equilibrium phase boundaries, Fig. 2(b) also shows analytical estimates for the metastability regions of the different phases (dashed lines). Transforming from a metastable to stable phase requires a nucleation event. Crossing the metastable boundaries is associated with the appearance of an unstable wavelength, which spontaneously triggers the phase change, as demonstrated below.

Along with the one-mode predictions, Fig. 2 shows direct simulation results. Simulations involving a periodic phase were initialized as a slab of one-mode approximation solid in contact with a uniform phase, at the predicted respective average densities. Density was evolved in a 200 by 2000 grid point box using Eq. (2) (discussed below) with a semi-implicit Fourier method, until convergence was reached [19]. Unless otherwise stated, the grid spacing $dx = a_0/10$ with a_0 the lattice constant, time step $dt = 1$,

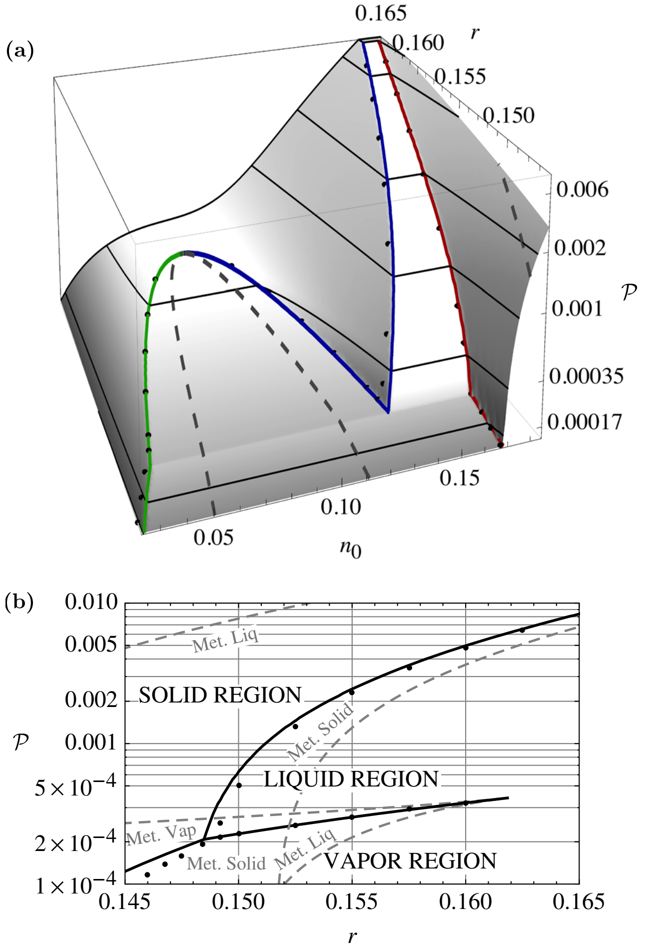

FIG. 2 (color online). (a) Density-temperature-pressure and (b) pressure-temperature phase diagrams of model. Solid thick lines correspond to one-mode calculations. In (a), green: vapor, blue: liquid, red: periodic coexistence values. Dashed line is the vapor-liquid spinodal. In (b), dashed lines show metastability regions. Black dots show average coexistence density [in (a)] or pressure [in (b)] from isothermal simulations. Model parameters as in Fig. 1.

$\lambda = 0.21$, and $\Gamma = 10$ (see figures for other parameters). Figure 2 shows that the coexistence densities [shown in Fig. 2(a)] and pressures [shown in Fig. 2(b)] from direct simulation are in excellent qualitative agreement with our analytical r-n_o-P and r-P space calculations, respectively. Deviations at low average density are in part due to finite size effects and due to surface energetics not captured in the phase diagram analysis.

To probe the three-phase kinetics at fixed volume, another simulation was performed where a uniform liquid was quenched into solid-vapor coexistence. The metastable liquid is seeded with a crystal, which grows [Fig. 3(a)]. As the solid depletes the surrounding liquid density, vapor pockets nucleate in high depletion areas [Fig. 3(b)]. Due to the different growth rates into liquid and vapor, long faceted solid branches are created [Fig. 3(c)], and the resulting structure is a seaweedlike dendrite [Fig. 3(d)].

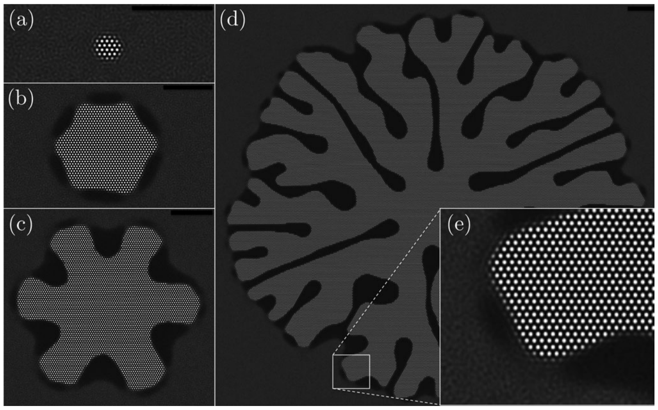

FIG. 3. Three-phase dendritic growth. A solid seed (periodic regions) grows into a metastable liquid (gray uniform areas). High depletion areas nucleate vapor pockets (black regions). See [19] for an animation. (a) $t = 100$, (b) $t = 4177$, (c) $t = 10293$, (d) $t = 36797$, (e) inset of (d). Scale bar: 20 lattice units. Model parameters: $a = 35$, $b = -12.01$, $c = 33.5$, $B_x = 0.3$, $n_0 = 0.125$, $N_a/(dx\sqrt{dt}) = 0.01$, $r = 0.145$.

Changes in system volume $V = dx^2 N_x N_y$ (for a 2D N_x by N_y grid) can be induced by modifying dx. As V changes, one also modifies the average density, n_o, so that $N = n_0 \cdot V$ remains constant. In practice, this is done by adding a uniform density flux J_V everywhere such as to recover the correct n_0.

To control the system pressure, we derived an equation of motion for the volume of the system, that is based on a control algorithm for $\omega' = -\Omega/V$, where Ω is the grand potential of the system. Applying the first law of thermodynamics to an infinitesimally small volume element, enclosed in a larger volume: $ds = (1/T)de - (\mu/T)d\rho + (P_0/(VT))dV$, where T is the temperature, μ the chemical potential, s the entropy density of the volume element, e its internal energy density, ρ the local number density, V the volume of the whole system, and P_0 is an externally imposed pressure. The natural variables of entropy are e, ρ, and V, and so changes in $\delta s/\delta e|_{\rho,V}$, $\delta s/\delta\rho|_{e,V}$, $\delta s/\delta V|_{e,\rho}$ drive the system. e and ρ obey conservation equations, but assuming an isothermal system, their evolution can be derived from a single density equation, i.e., of the form in Eq. (2). Volume V, considered as a dynamical variable, is a nonconserved global variable and therefore depends on all subelements. To linear order in the driving forces, $\frac{\partial V}{\partial t} = -M\int_V d\mathbf{r}[M_V(\partial s/\partial V) + M_e(\partial s/\partial e) + M_\rho(\partial s/\partial \rho)]$ where M_e, M_ρ and M_V are constants that depend on system variables (e, T, s, V, $\rho\ldots$), $1/M$ fixes the time scale of volume changes, while the integral over the system volume ensures a response only to global variations. Using the Gibbs relations, $-(\partial V/\partial t)/M = 1/V\int_V d\mathbf{r}\{M_V P_0 + V(M_e - M_\rho\mu)\}/T$. Stationarity, $\partial V/\partial t = 0$, implies that $V(M_e - M_\rho\mu)$ should be consistent with a pressure. This condition constrains the expressions for M_V, M_e, and M_ρ. We postulate that $M_V = 1/\bar{\rho}k_B$, $M_e = (e - Ts)/(\bar{\rho}k_B V^2) = f/(\bar{\rho}k_B V^2)$, and $M_\rho = \rho/(\bar{\rho}k_B V^2)$, so that the final evolution equation reads

$$\frac{\partial n}{\partial t} = \Gamma \nabla^2 \left(\frac{\delta \mathcal{F}}{\delta n}\right) + N_a \eta, \tag{2}$$

$$\frac{\partial V}{\partial t} = M(\omega - \mathcal{P}_0), \tag{3}$$

where $\omega = \int_V d\mathbf{r}(-f + \mu\rho)/(\bar{\rho} k_B T V)$ emerges as the adimensional functional generalization of ω' and $\mathcal{P}_0 = P_0/(\bar{\rho} k_B T)$. The noise η is a Gaussian stochastic variable which satisfies $\langle \eta(\mathbf{r}, t)\eta(\mathbf{r}', t')\rangle = -\nabla \cdot \nabla \delta(\mathbf{r} - \mathbf{r}')\delta(t - t')$, with N_a the noise amplitude. Equation (3) is effectively a simple control loop which increases or decreases the volume so that ω matches the externally imposed pressure $\mathcal{P}_0$, a barostat with time scale $1/M$.

In the absence of defects or interfaces, ω reduces to the thermodynamic pressure, but in complex bulk solids it additionally convolves interface and strain energies. To demonstrate our formalism, we only consider situations where, transient states aside, ω tracks pressure. In the particular case of seeded crystal growth simulations, interfaces are always present, and the ω integral is therefore restricted to a bulk region where density is uniform. In all constant pressure simulations, $M/(N_x N_y) = 2$ (unless otherwise stated), and where the average density increases (decreases), the initial grid spacing was respectively $dx = a_0/8$ $(dx = a_0/35)$.

Simulations of pressure induced transformation were first tested on vapor-liquid systems [Fig. 4(a)]. The initialization is done in either of the uniform phases and stabilized to an initial pressure over 5000 time steps, using Eqs. (2) and (3) with $\Gamma = 10$ on a 1008^2 grid. The target pressure $\mathcal{P}_0$ is then ramped up or down continuously, at a rate of $\pm 2.7027 \times 10^{-10}$. Because of fluctuations ($N_a/(dx\sqrt{dt}) = 0.01$), the starting phases stay metastable for as long as their compressibility stays positive, before spinodaly decomposing to the equilibrium phase [changes along orange lines in Figs. 4(a) and 4(a) inset (ii)]. To illustrate equilibrium transitions, metastable phases are seeded with the equilibrium phase (radius of 300 grid points), while pressure is monitored in the surrounding bulk. Pressure controlled growth follows [up or down arrows and Fig. 4(a) inset (i)]. Once the system is converted, it relaxes at a controlled average pressure.

The vapor-solid transition was tested in a similar manner [Fig. 4(b)]. Using $M/(N_x N_y) = 15$, the vapor phase pressure is continuously increased into the solid region, at a rate of 7.375×10^{-11} up to $\mathcal{P}_0 = 0.00012$ and then a rate of 2.48866×10^{-8} to $\mathcal{P}_0 = 0.01$. As the vapor crosses its metastability region, it spinodally decomposes to a liquid. The liquid then stays metastable until the crystal wavelength becomes unstable, spontaneously triggering another phase change into solid [lower orange line in Figs. 4(b), and 4(b) inset (ii)]. Equilibrium vapor-solid growth is induced by introducing a circular solid seed into the metastable vapor, just past the vapor-solid transition line [upward arrow and Fig. 4(b) inset (i)]. The seed first relaxes to a hexagon and controlling the vapor pressure then leads to a slow layered growth. If the target pressure is below the equilibrium vaporization temperature, the seed sublimates (downward arrow). Due to the absence of unstable boundaries, defects or noise, the bulk solid cannot be vaporized by under pressurizing it (topmost orange line). Well below the equilibrium vaporization point, vapor pockets can remain metastable for a long time due to pinning effects.

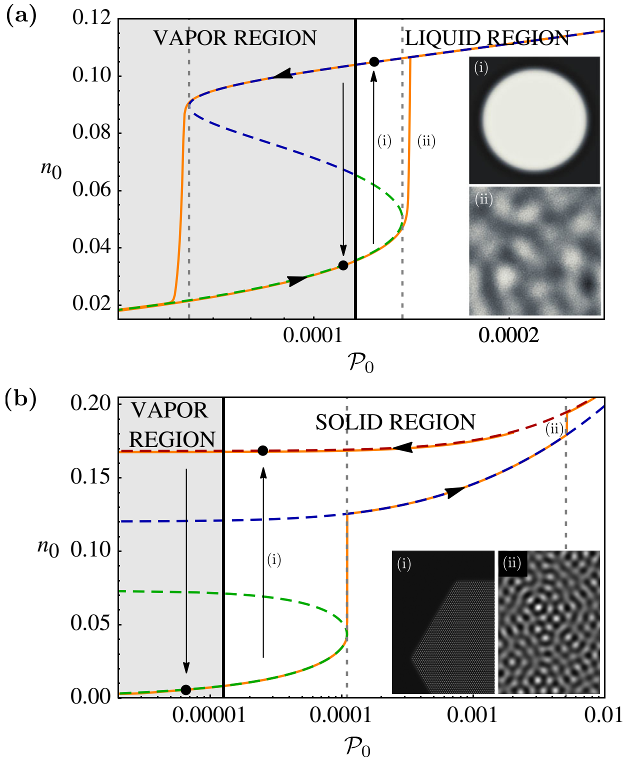

FIG. 4 (color online). Pressure controlled vapor-liquid [(a), $r = 0.155$] and vapor-solid [(b), $r = 0.147$] transformations. Thick vertical black line: equilibrium condensation or deposition point. Dashed green, blue, or red lines: average density vs pressure for vapor, liquid, or periodic phases. Continuous orange lines: system under pressure that is continuously increased or decreased (arrows show direction, $N_a/(dx\sqrt{dt}) = 0.01$). Vertical black arrows: seeded growth of a stable phase out of a metastable phase ($N_a/(dx\sqrt{dt}) = 0$). Insets show snapshots of the order parameter. Parameters as in Fig. 3.

The new formalism introduced here allows for novel, and experimentally relevant, applications in solid-vapor growth to be explored. Our theory captures the thermodynamics of pure substances excellently, while maintaining a fundamental connection with all elastoplastic properties of solids. The formalism introduced here offers new tools to model experimental processes in the fields of crystal growth (chemical vapor deposition or vapor-solid-liquid growth) or soft matter systems (phase separation in polymers, polymer crystals, or colloidal suspensions). In this Letter, we demonstrated how to control pressure by changing volume; it is straightforward to control pressure through density changes only, with a suitable replacement for Eq. (3). While purely technical issues still remain in regards to controlling pressure directly in complex bulk solids with interfaces and strain, this does not affect the theory. Future work will address the deconvolution of pressure from ω. One approach, for example, is to surround the system with a separate field describing an atmosphere.

The authors thank Nana Ofori-Opoku for useful discussions, The National Science and Engineering Research Council of Canada for funding and Compute Canada for HPC.

[1] K. R. Elder, M. Katakowski, M. Haataja, and M. Grant, Phys. Rev. Lett. **88**, 245701 (2002).

[2] H. Emmerich, H. Löwen, R. Wittkowski, T. Gruhn, G. I. Tóth, G. Tegze, and L. Gránásy, Adv. Phys. **61**, 665 (2012).

[3] M. Greenwood, N. Provatas, and J. Rottler, Phys. Rev. Lett. **105**, 045702 (2010).

[4] S. K. Mkhonta, K. R. Elder, and Z.-F. Huang, Phys. Rev. Lett. **111**, 035501 (2013).

[5] N. Ofori-Opoku, V. Fallah, M. Greenwood, S. Esmaeili, and N. Provatas, Phys. Rev. B **87**, 134105 (2013).

[6] J. Mellenthin, A. Karma, and M. Plapp, Phys. Rev. B **78**, 184110 (2008).

[7] J. Berry, N. Provatas, J. Rottler, and C. W. Sinclair, Phys. Rev. B **89**, 214117 (2014).

[8] J. Berry and M. Grant, Phys. Rev. Lett. **106**, 175702 (2011).

[9] E. J. Schwalbach, J. A. Warren, K.-A. Wu, and P. W. Voorhees, Phys. Rev. E **88**, 023306 (2013).

[10] T. V. Ramakrishnan and M. Yussouff, Phys. Rev. B **19**, 2775 (1979).

[11] A. J. Archer, J. Phys. Condens. Matter **18**, 5617 (2006).

[12] R. Evans, Adv. Phys. **28**, 143 (1979).

[13] K. R. Elder, N. Provatas, J. Berry, P. Stefanovic, and M. Grant, Phys. Rev. B **75**, 064107 (2007).

[14] Y. M. Jin and A. G. Khachaturyan, J. Appl. Phys. **100**, 013519 (2006).

[15] L. Gránásy, G. Tegze, G. I. Tóth, and T. Pusztai, Philos. Mag. **91**, 123 (2011).

[16] K.-A. Wu, A. Adland, and A. Karma, Phys. Rev. E **81**, 061601 (2010).

[17] M. Plischke and B. Bergersen, *Equilibrium Statistical Physics* (World Scientific, Singapore, 2006), 3rd ed.

[18] S. Walas, *Phase equilibria in chemical engineering* (Butterworth-Heinemann, Stoneham, 2013).

[19] See Supplemental Material at http://link.aps.org/supplemental/10.1103/PhysRevLett.114.155501, which includes Refs. [20,21]. It contains both a description of the numerical method, and an animation of the growth simulation shown in fig. 3.

[20] J. Berry, K. R. Elder, and M. Grant, Phys. Rev. E **77**, 061506 (2008).

[21] N. Provatas and K. Elder, *Phase-Field Methods in Materials Science and Engineering* (Wiley, Weinheim, 2010).